BIOCHEMISTRY
including biophysical chemistry & molecular biology

ARTICLE

pubs.acs.org/biochemistry

Semiquinone−Iron Complex of Photosystem II: EPR Signals Assigned to the Low-Field Edge of the Ground State Doublet of $Q_A^{\bullet-}Fe^{2+}$ and $Q_B^{\bullet-}Fe^{2+}$

Arezki Sedoud,[†] Nicholas Cox,[‡] Miwa Sugiura,[§] Wolfgang Lubitz,[‡] Alain Boussac,[†]
and A. William Rutherford*[,†,∥]

[†]iBiTec-S, CNRS URA 2096, CEA Saclay, 91191 Gif-sur-Yvette, France
[‡]MPI für Bioanorganische Chemie, Stiftstrasse 34-36, D-45470 Mülheim an der Ruhr, Germany
[§]Cell-Free Science and Technology Research Center, Ehime University, Bunkyo-cho, Matsuyama, Ehime 790-8577, Japan
[∥]Molecular Biosciences, Imperial College, London SW4 2AZ, U.K.

S *Supporting Information*

ABSTRACT: The quinone−iron complex of the electron acceptor complex of Photosystem II was studied by EPR spectroscopy in *Thermosynechococcus elongatus*. New $g \sim 2$ features belonging to the EPR signal of the semiquinone forms of the primary and secondary quinone, i.e., $Q_A^{\bullet-}Fe^{2+}$ and $Q_B^{\bullet-}Fe^{2+}$, respectively, are reported. In previous studies, these signals were missed because they were obscured by the EPR signal arising from the stable tyrosyl radical, $TyrD^{\bullet}$. When the $TyrD^{\bullet}$ signal was removed, either by chemical reduction or by the use of a mutant lacking TyrD, the new signals dominated the spectrum. For $Q_A^{\bullet-}Fe^{2+}$, the signal was formed by illumination at 77 K or by sodium dithionite reduction in the dark. For $Q_B^{\bullet-}Fe^{2+}$, the signal showed the characteristic period-of-two variations in its intensity when generated by a series of laser flashes. The new features showed relaxation characteristics comparable to those of the well-known features of the semiquinone−iron complexes and showed a temperature dependence consistent with an assignment to the low-field edge of the ground state doublet of the spin system. Spectral simulations are consistent with this assignment and with the current model of the spin system. The signal was also present in $Q_B^{\bullet-}Fe^{2+}$ in plant Photosystem II, but in plants, the signal was not detected in the $Q_A^{\bullet-}Fe^{2+}$ state.

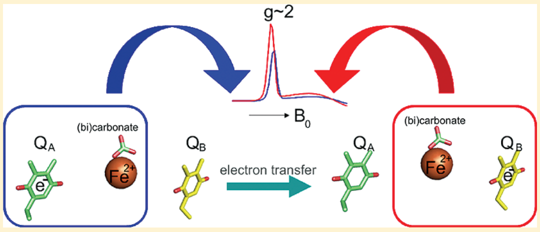

The electron acceptor complex of Photosystem II (PSII) involves two quinones, Q_A and Q_B, situated symmetrically on either side of a non-heme ferrous ion located at the level of the membrane−water interface of this intrinsic membrane−protein complex. Q_A is tightly bound and acts as a one-electron carrier, while Q_B undergoes two sequential one-electron reduction steps. Q_B is weakly bound in its quinone and quinol form but tightly bound in its one-electron-reduced semiquinone form (reviewed in ref 1). The non-heme iron is coordinated by four histidines and a bidentate carboxylic acid ligand.[1−3] In the homologous purple bacterial reaction center, this ligand is a glutamate of the M subunit,[4] while in PSII, it is a bicarbonate or carbonate ion.[4−7]

The proton-coupled electron transfer reactions that are associated with quinone reduction through the quinone−iron complex have been studied in great detail in purple bacterial reaction centers.[8,9] In PSII, however, these reactions remain relatively less well-known.[1] While many of the basic features of the purple bacterial reaction center are present in the quinone−iron complex of PSII, it seems likely that the different regulatory requirements specific to PSII have led to a range of structural and functional features that are not shared with its purple bacterial counterpart.

EPR spectroscopy can contribute to understanding the structure and function of the quinone−iron complex in PSII. As in the purple bacterial reaction center,[10] the semiquinone forms of both Q_A and Q_B can interact magnetically with the high-spin ferrous iron (Fe^{2+}, $S = 2$), producing similar but not identical EPR signals.[1,5] In native PSII, these signals are slightly shifted ($g \sim 1.9$ instead of $g \sim 1.8$) and have much weaker intensities.[11,12] In recent theoretical studies, this difference was attributed to the carboxylic acid ligand being carbonate rather than bicarbonate.[7] When bicarbonate or carbonate was replaced with formate, which unlike bicarbonate cannot undergo a second deprotonation, the EPR signals seen became almost indistinguishable from those naturally present in purple bacterial reaction centers.[13] Given the great enhancement of the intensity of these formate-modified signals, formate is often added to PSII to visualize the $Q_A^{\bullet-}Fe^{2+}$ signals (e.g., refs 14 and 15). Recently, we demonstrated that an equivalent formate-modified $Q_B^{\bullet-}Fe^{2+}$ signal can be formed.[16] This spectroscopic trick is useful, but nevertheless,

Received: March 1, 2011
Revised: May 30, 2011
Published: May 31, 2011

it represents a system that is inhibited and structurally modified by the non-native ligand.

In recent work from our laboratory, we noted a new EPR feature that seemed to be associated with the $Q_B^{\bullet-}$ state.[16,17] Here we report a study aimed at identifying this feature.

■ MATERIALS AND METHODS

Culture Conditions and PSII Preparation. The Photosystem II studied here was isolated from three different strains of *Thermosynechococcus elongatus* and from spinach. The three *T. elongatus* strains, all His-tagged on the CP43 subunit of PSII, were as follows: (1) WT, in which the *psbA$_1$* gene was dominantly expressed when grown under normal conditions;[18,19] (2) A3, a strain of cells in which the *psbA$_1$* and *psbA$_2$* genes were deleted so that only the *psbA$_3$* gene was expressed;[20] and (3) D2-Y160F, in which the tyrosine residue known as tyrosine D[21] was mutated to phenylalanine in the WT strain.[22] PSII core complexes were prepared using a protocol based on ref 23 with some modifications as described in ref 16. The oxygen evolution activities of the PSII core complexes isolated from the WT, A3, and D2-Y160F strains were as previously reported.[20,22,23] Samples were stored in liquid nitrogen in storage buffer [40 mM MES (pH 6.5), 15 mM $MgCl_2$, 15 mM $CaCl_2$, 1 M betaine, and 10% glycerol].

PSII-enriched membranes were isolated from market spinach as described in ref 24 with the following modification: bicarbonate was added at a final concentration of 1 mM to the thylakoid resuspension buffer, the solubilization buffer, and the storage buffer [25 mM MES (pH 6.5), 10 mM NaCl, 1 mM bicarbonate, and 0.3 M saccharose]. The oxygen evolution was ~600 μmol of O_2 (mg of Chl)$^{-1}$ h^{-1}. This isolation procedure was aimed at maintaining Q_B as functional as possible using milder detergent treatment[24] in the presence of bicarbonate.[25]

The presence of Q_B was verified by using thermoluminescence. A single flash produced the typical $S_2Q_B^{\bullet-}$ recombination band, and only a very small $S_2Q_A^{\bullet-}$ band was present. This indicates that Q_B is functional in the vast majority of centers.[26] Thermoluminescence was measured as described previously.[27]

Chemical Reduction Treatments. Chemical reduction of PSII with ascorbate was performed as follows. For both *T. elongatus* cores and PSII-enriched membranes from spinach, sodium ascorbate from a 300 mM stock solution in storage buffer was added to 120 μL of PSII (~1 mg of Chl/mL) in the EPR tube in darkness to give a final concentration of 10 mM. The *T. elongatus* sample was then incubated in darkness for 30 min at room temperature prior to being frozen. The PSII-enriched membrane sample was incubated for 60 min at room temperature prior to being frozen.

Dithionite reduction of *T. elongatus* PSII was performed at room temperature in darkness by addition of sodium dithionite to the sample in the EPR tube to give a final concentration of 2 mM using a 30 mM sodium dithionite stock solution made up in degassed storage buffer. The reduced sample was immediately frozen at 200 K in a solid CO_2/ethanol bath prior to EPR measurements.[28]

To eliminate EPR signals around the $g \sim 2$ region arising from free Mn^{2+} ions, EDTA (final concentration of 5 mM) was added to EPR samples used in this work, except for the experiments shown in Figures 2 and 3.

EPR Measurements. EPR spectra were recorded using a Bruker Elexsys 500 X-band spectrometer equipped with a standard ER 4102 resonator and Oxford Instruments ESR 900 cryostat. Instrument settings were as follows: microwave frequency, 9.4 GHz; modulation frequency, 100 kHz. All other settings were as indicated in the figure legends; 120 μL aliquots of PSII cores (~1 mg of Chl/mL) in the same buffer used for storage were loaded into 4 mm outer diameter quartz EPR tubes. The samples were manipulated under dim green light and then incubated in complete darkness for 12 h. For plant PSII, 120 μL aliquots of PSII-enriched membranes (~3 mg of Chl/mL) in the same buffer used for storage were loaded into 4 mm outer diameter quartz EPR tubes. The samples were manipulated under dim green light and then incubated in complete darkness for 2 h. The EPR samples were frozen in a solid CO_2/ethanol bath at 200 K. Samples were degassed by pumping (10^{-3} bar) at 200 K and then filled with helium gas. EPR tubes were then transferred to liquid nitrogen prior to the EPR measurements being made. Samples were handled in darkness.

The saturation curves were measured at 4 K after the tubes had been degassed at 200 K in a solid CO_2/ethanol bath. The fit used for the saturation curves to estimate the $P_{1/2}$ was as follows: SI = $a \times P^{1/2}/(1 + P/P_{1/2})^{b/2}$, where SI represents the signal intensity, a the normalization factor, P the microwave power, $P_{1/2}$ the half-saturating microwave power, and b the inhomogeneity factor.

The quantification of the contaminating radical signals was estimated by measuring the area of the double integral of the contaminating radical and comparing it with that of the total $TyrD^{\bullet}$ signal. The total $TyrD^{\bullet}$ was generated by illumination of the PSII sample at room temperature with room light (approximately 5 μE from white fluorescent room lights) for 1 min and then incubation for 20 s in the dark before the sample was frozen.

Illumination Conditions. Flash illumination was performed using a frequency-doubled Nd:YAG laser (Spectra Physics, 7 ns full width at half-maximum, 550 mJ, 532 nm) at room temperature. After a given number of saturating flashes, samples were rapidly frozen (1−2 s) in a solid CO_2/ethanol bath at 200 K followed by storage in liquid nitrogen. Low-temperature red-light illumination was performed in an unsilvered dewar containing liquid nitrogen (77 K). Illumination at 77 K was performed for 30 min to reduce Q_A and oxidize Cyt b_{559} to near completion, as verified by EPR. Continuous illumination with red light was performed by using an 800 W halogen lamp. The light was filtered through 3 cm of water, calflex IR heat filters, and a long-band-pass filter (RG-670 nm).

EPR Simulations. Spectral simulations were performed as described in ref 7. The spin Hamiltonian (10 × 10 matrix) was solved numerically using (i) Scilab-4.4.1, an open source vector-based linear algebra package (http://www.scilab.org), and (ii) the Easy Spin package[29] in MATLAB.

■ RESULTS

Illumination at 77 K. Figure 1a is a light-minus-dark difference spectrum induced by illumination at 77 K of *T. elongatus* (WT) PSII. Prior to recording the dark spectrum, we incubated the sample in the dark for 12 h. This incubation allowed the oxidation of $Q_B^{\bullet-}Fe^{2+}$ and the reduction of $TyrD^{\bullet}$ in a significant fraction of centers.[16,30] Sodium ascorbate (10 mM) was added 30 min before the end of the 12 h dark incubation to reduce Cyt b_{559} and the residual $TyrD^{\bullet}$. Illumination at 77 K is expected to result in the oxidation of Cyt b_{559} and the reduction of Q_A.[31] The near complete reduction of Cyt b_{559} by sodium ascorbate prior to illumination minimizes the appearance of Chl_Z/Car radical cation signals.[32−34] The TyrD does not undergo oxidation at

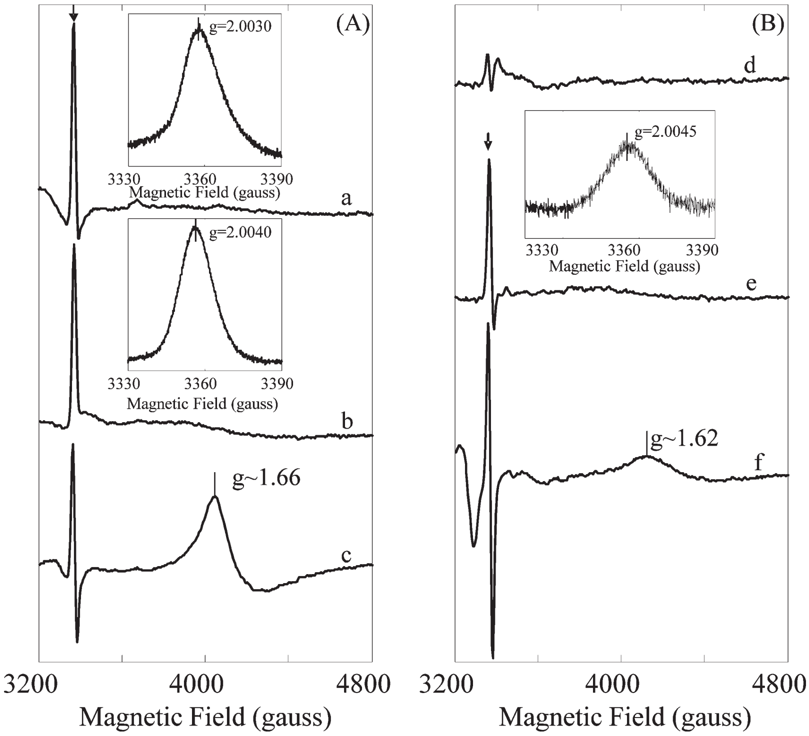

Figure 1. EPR signals attributed to $Q_A^{\bullet-}Fe^{2+}$ and $Q_B^{\bullet-}Fe^{2+}$ in PSII. Panel A shows spectra (a−c) of isolated *T. elongatus* WT PSII, while panel B shows spectra (d−f) of PSII-enriched membranes from spinach. PSII cores from WT *T. elongatus* were incubated in darkness for 11.5 h and then incubated with ascorbate (10 mM) for a further 30 min in darkness. PSII-enriched membranes from spinach were incubated for 2 h at room temperature and then incubated with ascorbate for 1 h in darkness (see Materials and Methods). Spectrum a is a 77 K illuminated-minus-dark spectrum of *T. elongatus* WT PSII attributed to $Q_A^{\bullet-}Fe^{2+}$. The top inset in panel A shows the $g \sim 2$ region of the 77 K illuminated-minus-dark spectrum on an expanded magnetic field scale and recorded at 160 mW. Spectrum b is a thawed-minus-dark spectrum attributed to $Q_B^{\bullet-}Fe^{2+}$ and obtained as follows. The 77 K illuminated sample used for spectrum a was warmed to room temperature, incubated for 10 min in darkness, and refrozen. The bottom inset in panel A shows the $g \sim 2$ region of the thawed-minus-dark $Q_B^{\bullet-}Fe^{2+}$ spectrum on an expanded field scale recorded at 160 mW. Spectrum c is a 77 K illuminated-minus-dark spectrum attributed to the $Q_A^{\bullet-}Fe^{2+}Q_B^{\bullet-}$ state, which was obtained when the sample containing $Q_B^{\bullet-}Fe^{2+}$ was reilluminated at 77 K. Spectrum d is a 77 K illuminated-minus-dark spectrum from plant PSII membranes attributed to the $Q_A^{\bullet-}Fe^{2+}$ state. To obtain this spectrum, the plant PSII sample was incubated in darkness for 30 min at 200 K after the 77 K illumination to allow the decay of P_{700}^{+} and F_A^{-}/F_B^{-} from contaminating PSI. Spectrum e is a thawed-minus-dark spectrum, attributed to plant $Q_B^{\bullet-}Fe^{2+}$. The inset in panel B shows the $g \sim 2$ region of the plant $Q_B^{\bullet-}Fe^{2+}$ signal recorded at 160 mW with an expanded magnetic field scale. Spectrum f is a 77 K illuminated-minus-dark spectrum attributed to the $Q_A^{\bullet-}Fe^{2+}Q_B^{\bullet-}$ state in plant PSII, obtained by reillumination of $Q_B^{\bullet-}Fe^{2+}$. The arrows show the new $g \sim 2$ features that are expanded in the insets. Instrument settings: microwave power, 20 mW; modulation amplitude, 25 G; temperature, 4 K. Instrument settings in the insets: microwave power, 160 mW; modulation amplitude, 10 G; temperature, 4 K.

this temperature at this pH.[35] Nevertheless, under these conditions, a signal is generated at $g \sim 2$ (Figure 1a). This signal is accompanied by the well-known broad signals at around 3400−4000 G that can be attributed to the $Q_A^{\bullet-}Fe^{2+}$ spin system.[7,11,30,36] The $g \sim 2$ signal is not a conventional first-derivative Gaussian signal typical of an organic free radical (see the top inset in Figure 1A); rather, it is a positive spike with a peak maximum at $g \sim 2.0030$ measured at 160 mW (see Effects of Microwave Power on the Field Position of the New Signals).

$Q_A^{\bullet-}$ to Q_B Electron Transfer. Electron transfer between $Q_A^{\bullet-}$ and Q_B is blocked at low temperatures (ref 37, and see ref 30 for a detailed study in *T. elongatus*). When a PSII sample, preilluminated at 77 K, is warmed to room temperature, forward electron transfer occurs,[26] and this is optimized when Cyt b_{559} is the electron donor, i.e., when Cyt b_{559} is fully reduced by ascorbate prior to illumination (see refs 16 and 30). Figure 1b is the $Q_B^{\bullet-}Fe^{2+}$ spectrum generated when the sample that had been illuminated at 77 K was thawed and incubated in the dark for 10 min. In this case, an intense $g \sim 2$ feature was also present. The new signal was even more clearly spikelike, and this small change in shape can be explained by the decay of the small underlying Chl/Car radical generated at 77 K when the sample was warmed (see ref 30). In the thawed sample, the peak position of the new signal was somewhat different, being at $g \sim 2.0040$ (bottom inset of Figure 1A; see also Effects of Microwave Power on the Field Position of the New Signals and Figure 4 for the power dependence of the peak position). The thawing procedure also produced changes in the broad signals that are ascribed to the replacement of $Q_A^{\bullet-}Fe^{2+}$ with $Q_B^{\bullet-}Fe^{2+}$, namely slight differences in signals around $g \sim 1.9$ and $g \sim 1.7$ (data not shown in detail here but see refs 16 and 30).

Biradical−Iron Complex ($Q_A^{\bullet-}Fe^{2+}Q_B^{\bullet-}$). When the sample containing $Q_B^{\bullet-}Fe^{2+}$ was reilluminated at 77 K, the $Q_A^{\bullet-}Fe^{2+}Q_B^{\bullet-}$ state was formed (Figure 1A, spectrum c), giving the characteristic $g \sim 1.66$ signal.[30,38] In addition, the $g \sim 2$ spike significantly decreased under these conditions, and the $g = 2$ signal became more radical-like. When it was measured under optimal conditions, we estimated that the radical EPR signal formed represented its presence in approximately 13% of the centers ($g = 2.0036$) (not shown). This is mainly attributable to

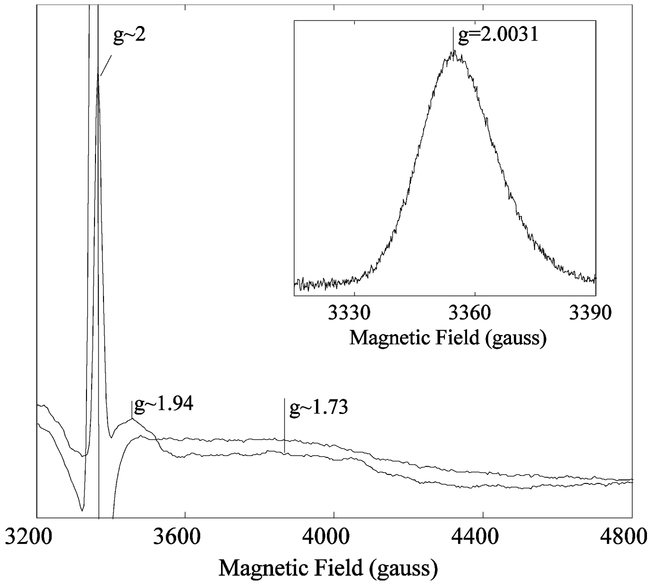

Figure 2. EPR signal attributed to $Q_A^{\bullet-}Fe^{2+}$ in *T. elongatus* PSII generated by reduction with sodium dithionite. Dark-adapted PSII without (broken line) and with (solid line) 2 mM dithionite frozen <1 min after dithionite addition. The inset shows the $g \sim 2$ region on an expanded field scale (recorded at 160 mW). The main *g* values are shown in the figure. Instrument settings: microwave power, 20 mW; modulation amplitude, 25 G; temperature, 5 K. Instrument settings for the inset: microwave power, 160 mW; modulation amplitude, 10 G; temperature, 4 K.

the Chl_Z/Car radical cations formed in the small fraction of centers in which Cyt b_{559} was oxidized prior to the illumination.

Plant PSII. Figure 1B shows an experiment similar to that in panel A except that the biological material was PSII-enriched membranes from spinach. The plant PSII-enriched membranes were adapted to darkness at room temperature for 2 h, and then ascorbate was added to reduce the Cyt b_{559} and $TyrD^{\bullet}$. This PSII preparation was based on a protocol aimed at maintaining Q_B integrity (see Materials and Methods), and one result of this is that there was some contamination by PSI. Illumination at 77 K thus resulted in formation of $P_{700}{}^{+}F_A{}^{-}/F_B{}^{-}$ in the PSI centers, and this charge pair is unstable at 200 K.[39] The Cyt $b_{559}{}^{ox}$ $Q_A^{\bullet-}Fe^{2+}$ charge pair in PSII is known to be stable at 200 K. Incubation of the sample at 200 K for 30 min in darkness allowed the magnitudes of the signals from PSI to diminish almost completely before the difference spectrum was recorded (Figure 1d). The light-minus-dark spectrum should then correspond to the $Q_A^{\bullet-}$ state in the presence of oxidized Cyt b_{559}. The spectrum obtained (Figure 1d) has the typical broad features of the $Q_A^{\bullet-}Fe^{2+}$ state, but it shows no obvious spike feature at $g \sim 2$. Given the difficulties with contributions of other radicals to the spectra before and after illumination, the exact spectrum in this region still remains unsure. Chemical reduction with dithionite also produces the $Q_A^{\bullet-}Fe^{2+}$ state (see the next section); however, in plant PSII, no spike signal that can be attributed to $Q_A^{\bullet-}Fe^{2+}$ could be seen upon addition of dithionite (not shown). Overall, it seems clear that a strong spike signal from $Q_A^{\bullet-}Fe^{2+}$, like that seen in *T. elongatus* under these conditions, is not present in plant PSII.

Spectrum e in Figure 1 shows the thawed-minus-dark difference spectrum of plant PSII-enriched membranes, corresponding to $Q_B^{\bullet-}Fe^{2+}$. Clearly, a $g \sim 2$ "spike" signal is present and similar to that seen in *T. elongatus* but with a *g* value of ~2.0045 when measured at 160 mW (see the inset in Figure 1B). When the experiment was conducted under the appropriate conditions, it was seen that the $Q_B^{\bullet-}Fe^{2+}$ spike is contaminated by a small $TyrD^{\bullet}$ radical signal (not shown). Spectrum f of Figure 1 shows that reillumination of this sample produced the $Q_A^{\bullet-}Fe^{2+}Q_B^{\bullet-}$ state showing a $g \sim 1.62$ signal. This *g* value is in agreement with the reported value for this state in plant PSII.[25] The formation of this signal confirms that $Q_B^{\bullet-}Fe^{2+}$ was present in this sample prior to the illumination at 77 K. In this case, spectrum f in Figure 1 is contaminated with the $P_{700}{}^{\bullet+}F_A{}^{\bullet-}/F_B{}^{\bullet-}$ charge pair. In this case, when a 200 K incubation in darkness was conducted to allow this charge pair to recombine, the amplitude of the $g \sim 1.62$ signal also decreased to some extent. This likely represents $Chl_Z{}^{+}Q_A^{\bullet-}$ recombination occurring in the presence of $Q_B^{\bullet-}$ and/or some forward electron transfer from $Q_A^{\bullet-}$ to $Q_B^{\bullet-}$ occurring during the 200 K incubation treatment.[30]

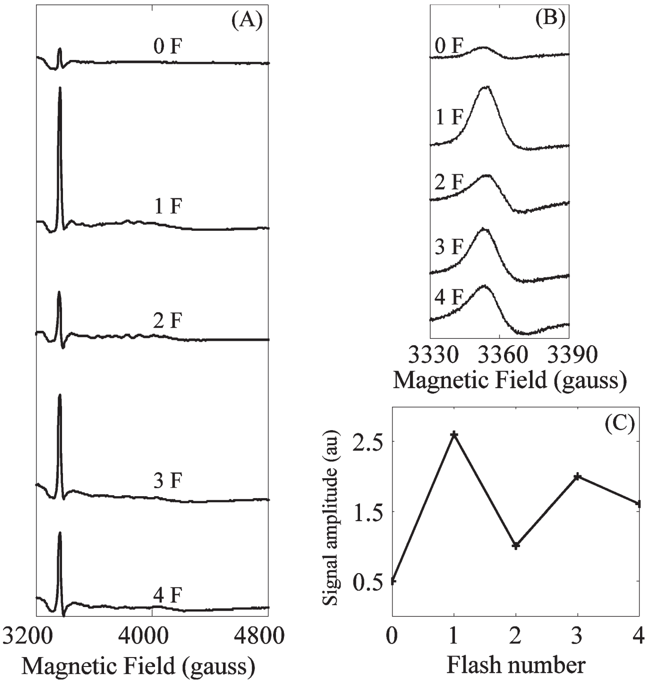

Figure 3. Flash number dependence of the intensity of the $g \sim 2$ EPR signal attributed to $Q_B^{\bullet-}Fe^{2+}$ in the TyrD-less mutant *T. elongatus* PSII. Samples were adapted to darkness for ~12 h, submitted to zero to four flashes at room temperature, and frozen rapidly. The resulting spectra are shown in panel A. Panel B shows the $g \sim 2$ region on an expanded magnetic field scale. Panel C shows a plot of the variation in intensity of the signal with flash number. Instrument settings for panel A: microwave power, 20 mW; modulation amplitude, 25 G; temperature, 4 K. Instrument settings for panel B: microwave power, 4 mW; modulation amplitude, 10 G.

Effect of Dithionite. The addition of sodium dithionite in the dark is expected to result in the formation of the $Q_A^{\bullet-}$ state in all the centers. Figure 2 shows that addition of sodium dithionite to PSII from *T. elongatus* generates the new signal along with the well-known $Q_A^{\bullet-}Fe^{2+}$ signals at $g \sim 1.9$ and $g \sim 1.73$. [The $g = 1.9$ signal has contributions from excited states and is optimally detected at higher temperatures, while the $g = 1.73$ signal is very broad and appears to be optimally detected at the lowest temperatures (see ref 7).] The generation of the new signal by dithionite is strong support for its assignment as $Q_A^{\bullet-}$.

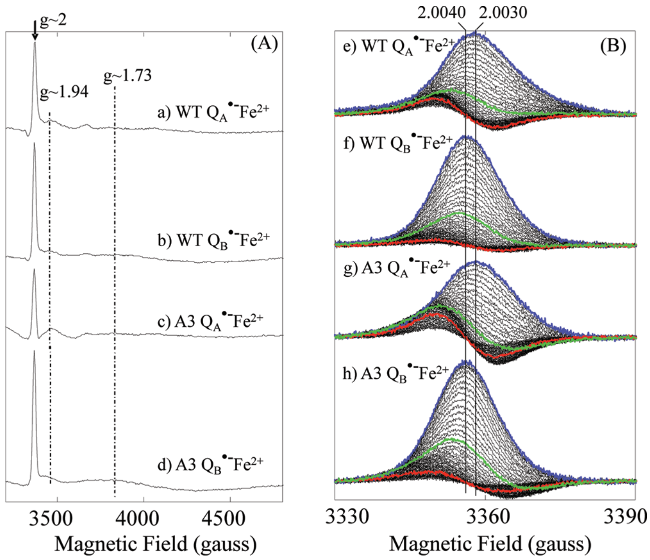

Figure 4. Comparison of the $Q_A^{\bullet-}Fe^{2+}$ and $Q_B^{\bullet-}Fe^{2+}$ EPR signals in PSII isolated from the WT and A3 strains of *T. elongatus*. Panel B shows the $g \sim 2$ region of the samples as shown in panel A on an expanded magnetic field scale. Spectra a (e) and c (g) show $Q_A^{\bullet-}Fe^{2+}$ in the WT and A3 strains, respectively. Spectra b (f) and d (h) show $Q_B^{\bullet-}Fe^{2+}$ in the WT and A3 strains, respectively. The $Q_A^{\bullet-}Fe^{2+}$ and $Q_B^{\bullet-}Fe^{2+}$ states were generated as described for Figure 1A. Panel B also shows the effect of microwave power on the difference spectra. The *g* values shown in panel B are those measured at 160 mW (blue spectrum). To illustrate the effects of microwave power on the shape and position of the spectra, a low-power (8 μW) spectrum is shown in red for each case, representing conditions under which the free radical signal is favored. At intermediate powers (e.g., 4 mW, highlighted in green), both the radical and the semiquinone−iron signals contribute. Instrument settings for panel A: microwave power, 20 mW; modulation amplitude, 25 G; temperature, 4 K. Instrument settings for panel B: modulation amplitude, 10 G; temperature, 4 K.

The spectrum in Figure 2 (solid line) is not a reduced-minus-oxidized difference spectrum. This is because dark adaption for 12 h still left $TyrD^{\bullet}$ in a significant fraction of centers prior to dithionite addition (note the intense radical signal present in the spectrum in Figure 2 shown by the dotted line). As expected, however, this radical signal was essentially eliminated by addition of dithionite (Figure 2, solid line). The inset shows a *g* value of the spike of ~2.0031 at 160 mW, a value similar to that obtained for light-induced $Q_A^{\bullet-}Fe^{2+}$ (Figure 1a).

The dithionite-induced $Q_A^{\bullet-}Fe^{2+}$ signal shown in Figure 2 demonstrates that the $g \sim 1.9$ feature, which is usually reported in samples containing $TyrD^{\bullet}$ and Chl_Z/Car cation radicals, is clipped at lower field by the radical (see, e.g., ref 30). In the absence of the radical, the peak of this feature appears at $g \sim 1.94$ at 5 K.

Effect of a Flash Series. To obtain further evidence of the assignment of the $g \sim 2$ signal to the $Q_B^{\bullet-}Fe^{2+}$ state, we looked for the mechanistic behavior typical of this component: the flash-number dependent, period-of-two variation of its intensity.[40,41] For this experiment, the tyrosine D-less mutant of *T. elongatus*[22] was used so that the new signal would not be swamped by the $TyrD^{\bullet}$ radical EPR signal. Figure 3A shows the result of the flash series given at room temperature using a sample incubated for 12 h in darkness to minimize the $Q_B^{\bullet-}$ population prior to flash illumination. The period-of-two variation in amplitude is evident, with larger signals on flashes 1 and 3 (Figure 3B,C). The pattern, however, was damped with only a small change occurring between flashes 3 and 4. This is to be expected in the isolated enzyme with no exogenous electron acceptor added. The fact that the changes occur on the third and fourth flashes is in line with our earlier observation that the isolated enzyme carries an additional functional quinone.[30] The data of Figure 3 constitute strong evidence that the new $g \sim 2$ signal arises from $Q_B^{\bullet-}$; taken with the evidence from Figure 1, this assignment can be considered definitive.

D1 Variants ($PsbA_1$ and $PsbA_3$). It is known that in *T. elongatus* there are three copies of the gene encoding the core reaction center subunit D1 (*psbA₁*, *psbA₂*, and *psbA₃*).[42] Under the growth conditions used here, only *psbA₁* is expressed.[18,43] There are 21 amino acid differences between $PsbA_1$ and $PsbA_3$; these confer small changes in the redox potentials of some cofactors.[18,44,45] In Figure 4A, we asked whether these structural changes are manifest as differences seen in the more complete spectra of the semiquinone−iron complex reported here. Both $Q_A^{\bullet-}Fe^{2+}$ and $Q_B^{\bullet-}Fe^{2+}$ have the same basic features: $g \sim 2$, $g \sim 1.9$, and $g \sim 1.7$. We note that $Q_A^{\bullet-}Fe^{2+}$ has a very small feature at $g \sim 1.8$ (most marked in Figure 4a), and this may be due to the loss of the native exchangeable carboxylate ligand, which has been suggested to be carbonate,[7] in a small fraction of centers. The spectra in Figure 4 show no significant difference between WT and the A_3 mutant in terms of their $Q_A^{\bullet-}Fe^{2+}$ and $Q_B^{\bullet-}Fe^{2+}$ EPR spectra, including the new signals.

Effects of Microwave Power on the Field Position of the New Signals. Figure 4B shows the dependence of the spectra on microwave power. At low powers, weak underlying radical signals are present (red spectra) and semiquinone−iron signals are not detectable. At high powers, the radical signals contribute very little to the spectra because they are highly oversaturated (Figure 4B, blue spectra). At intermediate powers (e.g., 4 mW, the green spectrum in Figure 4), mixtures of the two signals give apparent shifts in the peak position of the new $g \sim 2$ signals from $Q_A^{\bullet-}Fe^{2+}$ and $Q_B^{\bullet-}Fe^{2+}$. Where the contamination from underlying radical is greater, the effect on the peak position at intermediate powers (green spectra) is more marked (see Figure S1 of the Supporting Information). The *g* values of the new $Q_A^{\bullet-}Fe^{2+}$ and $Q_B^{\bullet-}Fe^{2+}$ signals were estimated at the highest microwave power used (160 mW), i.e., conditions under which the contributions of the $Q_A^{\bullet-}Fe^{2+}$ and $Q_B^{\bullet-}Fe^{2+}$ signals were maximal and those of the radical signals were minimal. The *g* values found for $Q_A^{\bullet-}Fe^{2+}$ and $Q_B^{\bullet-}Fe^{2+}$ were 2.0030 and 2.0040, respectively (blue in Figure 4B; see also the insets in Figures 1 and 2).

In Figure 4B, the underlying radical signal is larger in the $Q_A^{\bullet-}Fe^{2+}$ spectra than in the $Q_B^{\bullet-}Fe^{2+}$ spectra. This is expected because illumination at 77 K results in the formation of radicals from Chl_Z/Car generated in any centers in which Cyt b_{559} is unable to donate electrons.[31−33] This occurs in only a small fraction of centers because sodium ascorbate was added to the samples to reduce Cyt $b_{559\text{ox}}$. The *g* value measured for the radical signal is ~2.0040. This is higher than the expected value for the Chl_Z and Car radical cations.[31−33] This suggests that an additional radical species with a higher *g* value is also present in a small fraction of centers (see Discussion). Spin counting showed the total number of radicals formed by low-temperature illumination was ~10% of the concentration of PSII.

The Chl_Z/Car radicals decay when the sample is thawed. A residual signal is, however, present in $Q_B^{\bullet-}$-containing samples, and on the basis of its shape and *g* value, we attribute this signal to a small fraction of centers in which $TyrD^{\bullet}$ is formed (see Discussion).

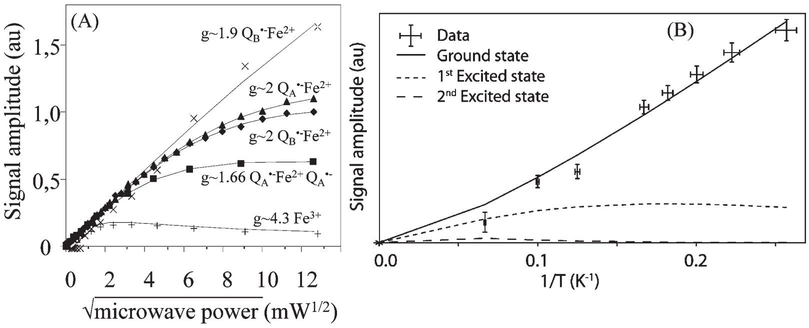

Figure 5. Microwave power saturation (A) and temperature dependence (B) of the $g \sim 2$ signals from the semiquinone−iron complex of WT *T. elongatus* PSII. In panel A, $g \sim 2$ signals from $Q_A^{\bullet-}Fe^{2+}$ (▲) and $Q_B^{\bullet-}Fe^{2+}$ (◆), $g \sim 1.9$ signals arising from $Q_B^{\bullet-}Fe^{2+}$ (×), the $g \sim 1.66$ signal arising from $Q_A^{\bullet-}Fe^{2+}Q_B^{\bullet-}$ (■), and the $g \sim 4.3$ signal from rhombic Fe^{3+} (+) are shown for comparison as controls. The lines were fitted to the data according to the equation described in Materials and Methods. $Q_B^{\bullet-}Fe^{2+}$ and $Q_A^{\bullet-}Fe^{2+}$ EPR signals were generated as described in the legend of Figure 1. Amplitudes of the signals were normalized at nonsaturating powers. For all the signals, the temperature was 4 K. The modulation amplitude was 25 G, except for the case of the $g \sim 2$ signals where the modulation amplitude was 10 G. In panel B, the $g \sim 2$ signal from $Q_B^{\bullet-}Fe^{2+}$ was measured at 4 mW, the modulation amplitude 10 G, and the temperature 4 K. The underlying radical was subtracted. The lines show the simulation of the temperature dependence of the $g \sim 2$ signal based on the spin Hamiltonian formalism (see eq 2). The solid line through the data represents the temperature dependence of the ground state of the semiquinone−iron manifold; higher states are shown with dashed lines. Fit parameters: $D = 16.6\ K^{-1}$ ($11.5\ cm^{-1}$), and $E/D = 0.25$.

Under the experimental conditions described in the legends of Figures 1 and 4, the $Q_A^{\bullet-}Fe^{2+}$ spectra have more radical contamination than those of $Q_B^{\bullet-}Fe^{2+}$ and the radical contaminants are different. This results in different effects as the microwave power is changed (Figure 4B). Plots of the field position of the new signal with microwave power show that the shift occurs at low powers and that it plateaus above 25 mW, with only relatively small changes occurring at higher powers (see Figure S1 of the Supporting Information). The size of the apparent field position shift with a change in the microwave power is dependent on the concentration and the spectral properties of the underlying radicals. The microwave power dependence of the apparent shift is related to the relaxation properties of the underlying radicals (see Figure S1 of the Supporting Information).

Microwave Power Saturation and Temperature Dependence. Figure 5A shows the saturation curves of the new $g \sim 2$ signals attributed to $Q_A^{\bullet-}Fe^{2+}$ and $Q_B^{\bullet-}Fe^{2+}$. Contributions from the underlying radicals were minimized by measuring the signal amplitudes at the magnetic field position corresponding to the crossing point for the free radicals. The relaxation properties of the new signals were compared to those of the $g \sim 1.9$ feature from $Q_B^{\bullet-}Fe^{2+}$, the $g \sim 1.66$ signal from $Q_A^{\bullet-}Fe^{2+}Q_B^{\bullet-}$, and, as a control, the $g \sim 4.3$ signal, which is generally attributed to a rhombic ferric iron contaminant commonly seen in biological systems. The intensities of the signals were normalized at nonsaturating powers.

The half-saturation $P_{1/2}$ value and the inhomogeneity factor, b, were found to be 75 mW and 1, respectively, for the $g \sim 2$ signal of $Q_A^{\bullet-}Fe^{2+}$ and 60 mW and 1.03, respectively, for the $g \sim 2$ signal of $Q_B^{\bullet-}Fe^{2+}$. The $g \sim 1.9$ signal of $Q_B^{\bullet-}Fe^{2+}$ did not reach saturation. The $g \sim 1.66$ signal of $Q_A^{\bullet-}Fe^{2+}Q_B^{\bullet-}$ had a $P_{1/2}$ value of 36 mW ($b = 1.27$). The $g \sim 4.3$ rhombic Fe^{3+} signal had a $P_{1/2}$ of 4 mW ($b = 1.50$). The new $g \sim 2$ signals had similar relaxation characteristics, and their saturation curves fell between the other fast relaxing species from the semiquinone−iron complex (i.e., the $g \sim 1.66$ and $g \sim 1.9$ signals). All of the signals associated with the semiquinone−iron complex saturated at much higher powers than the $g \sim 4.3$ rhombic iron signal. The fast relaxation properties of the new $g \sim 2$ signals are consistent with their attribution to the $Q_A^{\bullet-}Fe^{2+}$ and $Q_B^{\bullet-}Fe^{2+}$ states.

Figure 5B shows the temperature dependence of the $g \sim 2$ signal arising from $Q_B^{\bullet-}Fe^{2+}$. The $g \sim 2$ signal shows ground state behavior (see the next section for more details).

Simulations of the Spectra. Spectral simulations of the semiquinone−iron signal were performed using the spin Hamiltonian formalism. In earlier work, it has been shown that this approach is valid for all semiquinone−iron signals in the current literature.[7,10] A basis set that describes the non-heme iron ($S = 2$) semiquinone ($Q^{\bullet}$, $S_Q = {}^1/_2$) spin manifold can be built from the product of the eigenstates of the two interacting spins. These are expressed in terms of four quantum numbers: $|S_{Fe}\, m_{Fe}\, S_Q\, m_Q\rangle$, where S_{Fe} is the total spin of the ground state iron manifold ($S = 2$), m_{Fe} is the iron magnetic sublevel ($m = -S, -S + 1, ..., S - 1, S$), S_Q is the total spin semiquinone ($S = {}^1/_2$), and m_Q is the semiquinone sublevel ($m_Q = -{}^1/_2, {}^1/_2$). Thus, 10 basis vectors are required to span the spin manifold.

The spin Hamiltonian appropriate for the $Q_A^{\bullet-}Fe^{2+}$ system includes zero field (D and E), Zeeman (g_{Fe} and g_Q), and anisotropic exchange (J) terms:

$$\begin{aligned}\mathscr{H} &= D[(S_{FeZ}{}^2 - 1)/3S_{Fe}(S_{Fe} + 1) + (E/D)(S_{FeX}{}^2 - S_{FeY}{}^2)] \\ &\quad + \beta H\cdot \mathbf{g}_{Fe}\cdot S_{Fe} + \mathbf{g}_Q \beta HS - S_{Fe}\cdot \mathbf{J}\cdot S_Q \qquad (1)\end{aligned}$$

Subsequent calculations assume the zero-field, Zeeman iron, and exchange tensors to be colinear and $\mathbf{g}_Q$ to be scalar as in refs 7 and 10. Estimates for all the spin Hamiltonian parameters (D, E, $\mathbf{g}_{Fe}$, $\mathbf{g}_Q$, and J) have been made for the native "$g \sim 1.9$-type" semiquinone−iron signal: $D \sim 10\ cm^{-1}$ ($15\ K^{-1}$), and $E/D \sim 0.25$. The interaction between the quinone and the iron was axial and on the order of $\sim 0.5\ cm^{-1}$.

The semiquinone−iron signal can be understood as the intersection of two EPR signals that arise from the two lowest Kramers doublets of the quinone−iron spin manifold (for a full discussion, see ref 7). The ground Kramers doublet gives a broad EPR spectrum at magnetic fields above $g \sim 2$. The first excited state Kramers doublet instead appears at fields below $g \sim 2$ and has an approximately similar width in magnetic field space (see

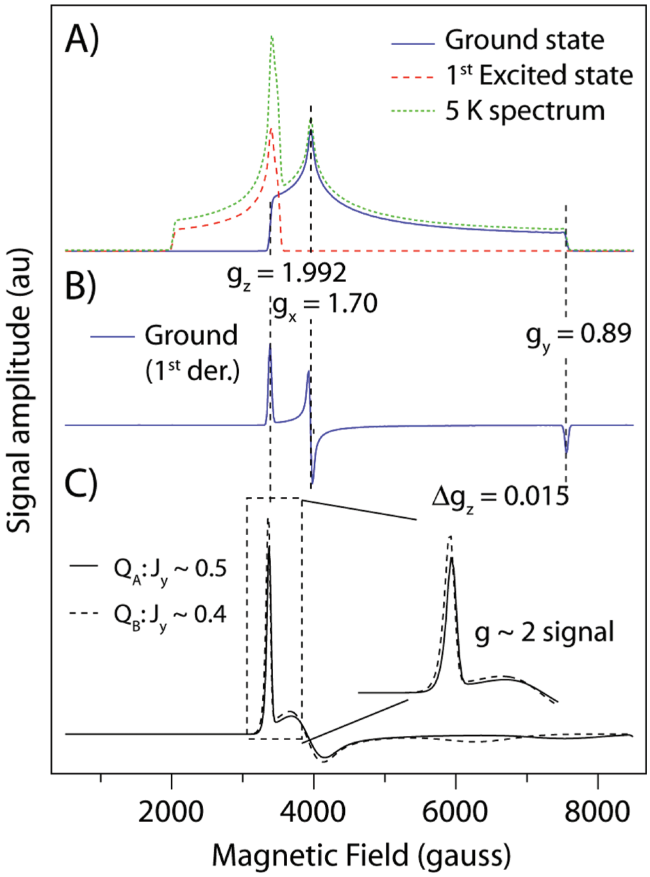

Figure 6. EPR simulation. (A) Simulation of the 5 K absorption line shape of the native semiquinone−iron signal in PSII using the spin Hamiltonian parameters reported in ref 7. (B) First-derivative line shape of the ground state component of the native semiquinone−iron signal as in panel A. (C) First-derivative line shape of the ground state component of the semiquinone−iron signal as presented in panel B allowing for anisotropic line broadening. The simulations shown in solid black and dashed black lines demonstrate that the exact position of $g_{\text{eff},z}$ is dependent on the magnitude of the component of the exchange coupling tensor along y ($\mathbf{J}_y$).

Figure 6A). A simple description of the system can be made where the two components (ground state and first excited state) of the EPR signal are described in terms of two effective spin = $^1/_2$ species (i = 1 or 2) of large g anisotropy.

$$\mathscr{H}_i = \beta H g_{\text{eff},i} S_i \qquad (2)$$

Analytical expressions for the effective g positions ($g_{\text{eff},x}$, $g_{\text{eff},y}$, and $g_{\text{eff},z}$) of the ground state and first excited state species in terms of the real spin Hamiltonian parameters (D, E, g_{Fe}, g_{Q}, and J) to third order are given in ref 10. Of the three effective g values, $g_{\text{eff},y}$ is unique and explains the characteristic line shape of all semiquinone−iron signals. It is the only g value that has a large first-order correction, such that $g_{\text{eff},y}$ decreases for the ground state ($g_{\text{eff},y} \sim 1$) and increases for the first excited state ($g_{\text{eff},y} \sim$ 3−4). This has the effect of spreading the signal across a very large magnetic field range (600 G) and explains why semiquinone−iron signals give only "weak" EPR signals. The approximate position of the $g_{\text{eff},y}$ ground and first excited state turning points scales with both the $\mathbf{J}_y$ component of the exchange coupling tensor and zero-field splitting parameters of the Fe^{2+}. This is in contrast to the other two effective g values, $g_{\text{eff},x}$ and $g_{\text{eff},z}$. The first-order corrections to these turning points are small, and as such that they are both approximately 2.0. The dependence of $g_{\text{eff},x}$ and $g_{\text{eff},z}$ on the spin Hamiltonian parameters (D, E, g_{Fe}, g_{Q}, and J) is, as a consequence, far more complicated.

Figure 6A shows the current model for the two lowest doublets of the native $g \sim 1.9$-type semiquinone−iron signal based on the spin Hamiltonian formalism described above.[7] In this model, the ground doublet $g_{\text{eff},x}$ defines the broad $g \sim 1.7$ turning point, whereas $g_{\text{eff},z}/g_{\text{eff},x}$ turning points of the first excited state doublet dominantly define the characteristic $g \sim 1.9$ turning point. It is for this reason that the semiquinone−iron signal of PSII is actually more readily observed at higher temperatures than its purple bacterial counterpart, which exhibits a $g \sim 1.8$-type semiquinone−iron spectrum.[7] Within this model, a rationale for the $g \sim 2$ spike can be immediately proposed: it is consistent with the remaining unassigned turning point, i.e., that of the ground doublet $g_{\text{eff},z}$. This assignment is also consistent with the temperature dependence of the $g \sim 2$ spike; its intensity increases as the temperature decreases. In a previous publication,[7] we estimated the fine structure parameters of the Fe^{2+} ion, which define the zero-field splitting of the quinone−iron complex and thus the temperature dependence of its EPR signal. These values were estimated to be as follows: $D = 15\ \text{K}^{-1}$, and $E/D = 0.25$. A fitting of the temperature dependence of the $g \sim 2$ spike yields similar results: $D = 16.6\ \text{K}^{-1}$, and $E/D = 0.25$.

When the ground doublet is viewed as the first derivative of the EPR absorption profile (Figure 6B), indeed a positive spike is present just as observed experimentally. To reproduce this spike, however, the effective line width along the principle z axis had to be significantly reduced relative to that along the x and y axes. If this is not included in these simulations, then the ground doublet $g_{\text{eff},z}$ turning point is effectively buried under the first excited state doublet as suggested by Figure 6A. This though is the only modification that had to be made to the simulations of Cox et al.[7] to generate the new feature. The simulation as presented in Figure 6C is only of the ground state and as such approximates the 5 K EPR spectrum. Here the $g \sim 1.7$ turning point is seen along with the $g \sim 2$ spike. The inclusion of the first excited state is necessary, however, to reproduce the other features in the field region around 3600−4000 G (the well-known $g \sim 1.9$ signal).

The exact position of the ground state $g_{\text{eff},z}$ is sensitive to the changes in the exchange coupling tensor $\mathbf{J}$. Only a small change in the $\mathbf{J}_y$ component ($0.1−0.2\ \text{K}^{-1}$) of the exchange coupling tensor is sufficient to shift the position of the $g \sim 2$ spike over the range of values seen for $\text{Q}_\text{A}^{\bullet-}\text{Fe}^{2+}$ and $\text{Q}_\text{B}^{\bullet-}\text{Fe}^{2+}$ signals (2.0030−2.0040). This is not the case for $\mathbf{J}_z$ and $\mathbf{J}_x$. The position of $g_{\text{eff},z}$ is insensitive to small changes in $\mathbf{J}_z$. Similarly, while $\mathbf{J}_x$ does alter the position of $g_{\text{eff},z}$, these changes also lead to modifications of the other turning points: the ground state $g_{\text{eff},x}$ ($g \sim 1.7$) and excited state turning points ($g_{\text{eff},x}/g_{\text{eff},z}$, $g \sim 1.9$), etc., the characteristic EPR signals observed for the semiquinone−iron complex. It is thus likely that the small difference seen between the $g \sim 2$ spike for the $\text{Q}_\text{A}^{\bullet-}\text{Fe}^{2+}$ and $\text{Q}_\text{B}^{\bullet-}\text{Fe}^{2+}$ signals most probably reflects small changes in $\mathbf{J}_y$, possibly the rotation of the exchange tensor in the $\mathbf{J}_y/\mathbf{J}_z$ plane relative to the fine structure tensor of the Fe^{2+}. Small tensor rotations of this magnitude were inferred to explain the variations found within the set of $g \sim 1.8$-type semiquinone−iron signals, i.e., those seen in PSII when formate is present and in native purple bacterial reaction centers.[7] It is noted that small differences between the $\text{Q}_\text{A}^{\bullet-}\text{Fe}^{2+}$ and

$Q_B^{\bullet-}Fe^{2+}$ $g \sim 2$ spike signals must be related to the exchange tensor as opposed to the fine-structure tensor/**g** tensor of the Fe^{2+}. The Fe^{2+} is the same for both complexes.

The EPR line width parameter used for the EPR simulations (Figure 6C) must be highly anisotropic to reproduce a "sharp" $g_{\mathrm{eff},z}$ spike at $g \sim 2$ and relatively broad turning points at $g \sim 1.9$, $g \sim 1.7$, etc. It is interesting to note that the apparent EPR line width along the three principal axes (x, y, and z) would appear to correlate with the magnitude of the exchange coupling along the three principal directions; the coupling and the line width are small along z, whereas the coupling and line width are large along x and y.

■ DISCUSSION

In this work, we have identified an additional feature of the EPR signal arising from the magnetic interaction of the semiquinone with the non-heme high-spin (Fe^{2+}, $S = 2$) ferrous iron on the electron acceptor side of PSII. Both $Q_A^{\bullet-}Fe^{2+}$ and $Q_B^{\bullet-}Fe^{2+}$ EPR signals include a sharp $g \sim 2$ feature with slightly differing g values (2.0030 and 2.0040 for $Q_A^{\bullet-}Fe^{2+}$ and $Q_B^{\bullet-}Fe^{2+}$, respectively). The lines of evidence for the assignment of the signals are as follows. (i) The new feature associated with $Q_A^{\bullet-}Fe^{2+}$ is generated by illumination at 77 K and by reduction with sodium dithionite in darkness, i.e., standard conditions for the formation of $Q_A^{\bullet-}$. (ii) The new signal associated with $Q_B^{\bullet-}Fe^{2+}$ is formed (a) upon thawing a sample containing $Q_A^{\bullet-}Fe^{2+}$ and (b) upon flash illumination at room temperature, it being bigger on the first and third flashes. These conditions correspond to those in which $Q_B^{\bullet-}Fe^{2+}$ is formed. (iii) The new features have relaxation properties similar to those of the other signals arising from the semiquinone−iron complex.

In two recent papers from our lab, we made observations that also support the assignment of the $g \sim 2$ signal to $Q_B^{\bullet-}Fe^{2+}$. We noted that the $g \sim 2$ feature was present when $Q_B^{\bullet-}Fe^{2+}$ was generated by a chemical reduction (DAD/ascorbate) and the $g \sim 2$ feature disappeared when the sample was illuminated at 77 K upon formation of the $Q_A^{\bullet-}Fe^{2+}Q_B^{\bullet-}$ state.[16] In addition, the spike signal was found to be present in ∼50% of centers after dark adaptation for 1 h in the TyrD-less mutant of *T. elongatus* and disappeared, along with the $g \sim 1.94$ feature, when an artificial electron acceptor was added. This behavior fits with that expected of $Q_B^{\bullet-}Fe^{2+}$.[17]

The new features observed here are relatively narrow and thus relatively intense, yet they have escaped detection until now. This is because the EPR signal from $\mathrm{TyrD}^{\bullet}$ is considerably larger than the new signals and it obscures this region of the spectrum. In this work we were able to circumvent these problems by the use of reducing agents or the TyrD-less mutant to eliminate contributions of $\mathrm{TyrD}^{\bullet}$ to the spectra. In addition, until relatively recently, most of the work on the acceptor side of PSII was conducted with PSII-enriched membranes from plants, and here we observed that $Q_A^{\bullet-}Fe^{2+}$ has no (or a significantly smaller) $g \sim 2$ feature. In addition, the light-induced generation of the $Q_A^{\bullet-}Fe^{2+}$ signal at low temperatures is usually accompanied by the formation of variable amounts of $\mathrm{Chl_Z}$/Car radical cation signals,[32−34,46] and these also obscure the new photogenerated $Q_A^{\bullet-}Fe^{2+}$ feature at $g \sim 2$. Here we used sodium ascorbate to reduce any oxidized Cyt b_{559} prior to illumination to minimize the formation of these side path radicals.

We found that a small fraction of centers exhibited a free radical signal even when efforts had been made to avoid contaminating radicals. This was particularly evident in the relaxation studies (Figure 4B). The identity of the radical signals under the various experimental conditions can be suggested.

In the dithionite-reduced $Q_A^{\bullet-}Fe^{2+}$ spectrum, a radical with a g value of 2.0044 was present, and given the low level of resolved hyperfine splitting (not shown), we suggest that this could reflect a small fraction of centers in which the semiquinone is uncoupled from the non-heme iron and possibly a small contribution from unreduced $\mathrm{TyrD}^{\bullet}$. The total number of centers contributing to the radical signal was approximately 4%. It is well-known that the semiquinone can be uncoupled from the iron using a range of biochemical treatments.[47−51] One of these methods was no more than washing a cyanobacterial core prep with phosphate buffer.[51] Because the histidine-tagged preparation picks up PSII in several phases of its life cycle, it is possible that a subpopulation could be present that lacks the high-spin iron or is prone to losing it during the preparation.

Without dithionite, the contaminating radical signal in the photogenerated $Q_A^{\bullet-}Fe^{2+}$ is expected to be due to the side path radicals ($\mathrm{Chl_Z}$ and Car) formed in the residual centers in which Cyt b_{559} is oxidized prior to illumination. However, the g value for the radical signal was 2.0040, a value that is too high for the side path radicals alone.[32,34] We attribute this to a mixture of side path radicals, a small fraction of uncoupled $Q_A^{\bullet-}$, and perhaps some $\mathrm{TyrD}^{\bullet}$. The number of centers showing a radical is estimated to be approximately 10%. When $Q_B^{\bullet-}Fe^{2+}$ is formed, the radical contamination with a g value of 2.0044 is attributed to a small fraction of $\mathrm{TyrD}^{\bullet}$, and we do not rule out a possible contribution from a fraction of uncoupled $Q_B^{\bullet-}$. The mechanism of formation of $\mathrm{TyrD}^{\bullet}$ is most likely as follows. The $\mathrm{Mn_4Ca}$ cluster undergoes oxidation in 5−10% of the centers upon illumination at 77 K,[26] and then upon thawing, TyrD donates electrons to S_2 at room temperature forming $\mathrm{TyrD}^{\bullet}$ (reviewed in ref 21). The ascorbate in the sample slowly reduces the $\mathrm{TyrD}^{\bullet}$, but this is incomplete under the conditions used in our experiment. The quantitation of the radical indicates approximately 5% of centers exhibit the radical signal under these conditions.

As already mentioned, the g value of the new signal from $Q_A^{\bullet-}Fe^{2+}$ is ∼2.0030, while that of $Q_B^{\bullet-}Fe^{2+}$ is ∼2.0040. These values were obtained at 160 mW. At lower microwave powers, the field position of the peak appears to change, but this is clearly caused by the presence of the underlying free radical signals that are favored at low microwave powers. In *T. elongatus*, the new signal appeared to be slightly stronger in $Q_B^{\bullet-}Fe^{2+}$ than in $Q_A^{\bullet-}Fe^{2+}$. In plant PSII, while the signal is clearly present in the $Q_B^{\bullet-}Fe^{2+}$ state (with a slightly different position, at $g \sim 2.0045$), it is very weak or absent in $Q_A^{\bullet-}Fe^{2+}$. The significance of this observation has yet to be understood; however, it does seem to constitute a specific species difference.

The small spectral differences between $Q_A^{\bullet-}Fe^{2+}$ and $Q_B^{\bullet-}Fe^{2+}$ seen here in *T. elongatus* reflect a small difference in the environment of the two semiquinones related to their different structural and functional properties. We were, however, unable to detect differences in the continuous wave EPR signals from $Q_A^{\bullet-}Fe^{2+}$ and $Q_B^{\bullet-}Fe^{2+}$ upon comparison of PSII from the WT ($\mathrm{PsbA_1}$) and A_3 ($\mathrm{PsbA_3}$) strains.

The temperature dependence of the new $g \sim 2$ signal indicates that it arises from a ground state. Within the context of the current model[7,10] and given the spike-type feature in the first-derivative spectrum, these signals would appear to be directly attributable to the low-field edge of the ground state doublet. This is confirmed by the spectral simulations. The new feature provides additional restrictions to the simulation parameters, and it also shows that the model used and the values obtained by Cox et al. were valid.[7] The decrease in the intensity of the signal when the $Q_A^{\bullet -}Fe^{2+}Q_B^{\bullet -}$ state is formed is in agreement with our ongoing attempts to simulate the EPR spectrum from this state (N. Cox et al., manuscript in preparation).

The signals from $Q_A^{\bullet -}Fe^{2+}$ and $Q_B^{\bullet -}Fe^{2+}$ in PSII reported here add to the spectroscopic probes with which we can study this enzyme. The strong intensity of the new signals should allow studies to be undertaken that were not previously feasible.

■ ASSOCIATED CONTENT

S Supporting Information. Marked effects of microwave power of the field position of the new semiquinone—iron signals shown in more detail and effects of lower field modulation, lower microwave power, and higher temperature on the signal shape. This material is available free of charge via the Internet at http://pubs.acs.org.

■ AUTHOR INFORMATION

Corresponding Author

*iBiTec-S, CNRS URA 2096, CEA Saclay, 91191 Gif-sur-Yvette, France, and Molecular Biosciences, Imperial College, London SW4 2AZ, U.K. Telephone: +33 1 69 08 2940. Fax: + 33 1 69 08 87 17. E-mail: alfred.rutherford@cea.fr.

Funding Sources

This work was supported by the EU/Energy Network Project SOLAR-H2 (FP7 Contract 212508). A.B. and M.S. were supported by the JSPS and CNRS under the Japan-France Research Cooperative Program, via a Grant-in-Aid for Scientific Research from the Ministry of Education, Science, Sports, Culture and Technology (21612007 to M.S.). A.S. was supported by the IRTELIS training program of the CEA.

■ ACKNOWLEDGMENT

We thank A. Krieger-Liszkay and D. Kirilovsky for helpful discussion.

■ ABBREVIATIONS

Car, carotenoid; Chl, chlorophyll; Cyt b_{559}, cytochrome b_{559}; EPR, electron paramagnetic resonance; PSII, Photosystem II; Q_A and Q_B, primary and secondary quinone electron acceptors, respectively, of PSII; TyrD, stable tyrosyl radical.

■ REFERENCES

(1) Petrouleas, V., and Crofts, A. R. (2005) The iron-quinone acceptor complex. In *Photosystem II. The light-driven water:plastoquinone oxidoreductase* (Wydrzynski, T., and Satoh, K., Eds.) pp 177—206, Springer, Dordrecht, The Netherlands.

(2) Ferreira, K. N., Iverson, T. M., Maghlaoui, K., Barber, J., and Iwata, S. (2004) Architecture of the photosynthetic oxygen-evolving center. *Science 303*, 1831–1838.

(3) Guskov, A., Kern, J., Gabdulkhakov, A., Broser, M., Zouni, A., and Saenger, W. (2009) Cyanobacterial photosystem II at 2.9-angstrom resolution and the role of quinones, lipids, channels and chloride. *Nat. Struct. Mol. Biol. 16*, 334–342.

(4) Michel, H., and Deisenhofer, J. (1988) Relevance of the photosynthetic reaction center from purple bacteria to the structure of Photosystem II. *Biochemistry 27*, 1–7.

(5) Rutherford, A. W. (1987) How close is the analogy between the reaction center of PSll and that of purple bacteria? 2. The electron acceptor side. In *Progress in Photosynthesis Research* (Biggins, J., Ed.) pp 277—283, Martinus Nijhoff, Dordrecht, The Netherlands.

(6) Hienerwadel, R., and Berthomieu, C. (1995) Bicarbonate binding to the non-heme iron of photosystem II investigated by Fourier transform infrared difference spectroscopy and C-13-labeled bicarbonate. *Biochemistry 34*, 16288–16297.

(7) Cox, N., Jin, L., Jaszewski, A., Smith, P. J., Krausz, E., Rutherford, A. W., and Pace, R. (2009) The semiquinone-iron complex of Photosystem II: Structural insights from ESR and theoretical simulation; evidence that the native ligand to the non-heme iron is carbonate. *Biophys. J. 97*, 2024–2033.

(8) Wraight, C. A. (2004) Proton and electron transfer in the acceptor quinone complex of photosynthetic reaction centers from *Rhodobacter sphaeroides. Front. Biosci. 9*, 309–337.

(9) Okamura, M. Y., Paddock, M. L., Graige, M. S., and Feher, G. (2000) Proton and electron transfer in bacterial reaction centers. *Biochim. Biophys. Acta 1458*, 148–163.

(10) Butler, W. F., Calvo, R., Fredkin, D. R., Isaacson, R. A., Okamura, M. Y., and Feher, G. (1984) The electronic-structure of Fe^{2+} in reaction centers from *Rhodopseudomonas sphaeroides*. 3. Electron-Paramagnetic-Res measurements of the reduced acceptor complex. *Biophys. J. 45*, 947–973.

(11) Rutherford, A. W., and Zimmermann, J. L. (1984) A new Electron-Paramagnetic-Res signal attributed to the primary plastosemiquinone acceptor in Photosystem-II. *Biochim. Biophys. Acta 767*, 168–175.

(12) Zimmermann, J. L., and Rutherford, A. W. (1986) Photoreductant-induced oxidation of Fe^{2+} in the electron-acceptor complex of Photosystem-II. *Biochim. Biophys. Acta 851*, 416–423.

(13) Vermaas, W. F. J., and Rutherford, A. W. (1984) Electron-paramagnetic-res measurements on the effects of bicarbonate and triazine resistance on the acceptor side of Photosystem-II. *FEBS Lett. 175*, 243–248.

(14) van Mieghem, F., Brettel, K., Hillmann, B., Kamlowski, A., Rutherford, A. W., and Schlodder, E. (1995) Charge recombination reactions in Photosystem-II. 1. Yields, recombination pathways, and kinetics of the primary pair. *Biochemistry 34*, 4798–4813.

(15) Mamedov, F., Nowaczyk, M. M., Thapper, A., Rogner, M., and Styring, S. (2007) Functional characterization of monomeric photosystem II core preparations from *Thermosynechococcus elongatus* with or without the Psb27 protein. *Biochemistry 46*, 5542–5551.

(16) Sedoud, A., Kastner, L., Cox, N., El-Alaoui, S., Kirilovsky, D., and Rutherford, A. W. (2011) Effects of formate binding on the quinone-iron electron acceptor complex of photosystem II. *Biochim. Biophys. Acta 1807*, 216–226.

(17) Boussac, A., Sugiura, M., and Rappaport, F. (2011) Probing the quinone binding site of Photosystem II from *Thermosynechococcus elongatus* containing either PsbA1 or PsbA3 as the D1 protein through the binding characteristics of herbicides. *Biochim. Biophys. Acta 1807*, 119–129.

(18) Sugiura, M., Kato, Y., Takahashi, R., Suzuki, H., Watanabe, T., Noguchi, T., Rappaport, F., and Boussac, A. (2010) Energetics in Photosystem II from *Thermosynechococcus elongatus* with a D1 protein encoded by either the *psbA1* or *psbA3* gene. *Biochim. Biophys. Acta 1797*, 1491–1499.

(19) Hughes, J. L., Rutherford, A. W., Sugiura, M., and Krausz, E. (2008) Quantum efficiency distributions of photo-induced side-pathway donor oxidation at cryogenic temperature in photosystem II. *Photosynth. Res. 98*, 199–206.

(20) Sugiura, M., Boussac, A., Noguchi, T., and Rappaport, F. (2008) Influence of histidine-198 of the D1 subunit on the properties of the primary electron donor, P680, of photosystem II in *Thermosynechococcus elongatus. Biochim. Biophys. Acta 1777*, 331–342.

(21) Rutherford, A. W., Boussac, A., and Faller, P. (2004) The stable tyrosyl radical in Photosystem II: Why D? *Biochim. Biophys. Acta 1655*, 222–230.

(22) Sugiura, M., Rappaport, F., Brettel, K., Noguchi, T., Rutherford, A. W., and Boussac, A. (2004) Site-directed mutagenesis of *Thermosynechococcus elongatus* photosystem II: The O_2-evolving enzyme lacking the redox-active tyrosine D. *Biochemistry 43*, 13549–13563.

(23) Sugiura, M., and Inoue, Y. (1999) Highly purified thermostable oxygen-evolving photosystem II core complex from the thermophilic cyanobacterium *Synechococcus elongatus* having his-tagged CP43. *Plant Cell Physiol. 40*, 1219–1231.

(24) Johnson, G. N., Boussac, A., and Rutherford, A. W. (1994) The origin of 40−50°C thermoluminescence bands in Photosystem-II. *Biochim. Biophys. Acta 1184*, 85–92.

(25) Hallahan, B., Ruffle, S., Bowden, S., and Nugent, J. H. A. (1991) Identification and characterization of EPR signals involving Q_B semiquinone in plant Photosystem-II. *Biochim. Biophys. Acta 1059*, 181–188.

(26) Rutherford, A. W., Crofts, A. R., and Inoue, Y. (1982) Thermoluminescence as a probe of Photosystem-II photochemistry: The origin of the flash-induced glow peaks. *Biochim. Biophys. Acta 682*, 457–465.

(27) Ishida, N., Sugiura, M., Rappaport, F., Lai, T. L., Rutherford, A. W., and Boussac, A. (2008) Biosynthetic exchange of bromide for chloride and strontium for calcium in the photosystem II oxygen-evolving enzymes. *J. Biol. Chem. 283*, 13330–13340.

(28) Boussac, A., Un, S., Horner, O., and Rutherford, A. W. (1998) High-spin states ($S \geq 5/2$) of the photosystem II manganese complex. *Biochemistry 37*, 4001–4007.

(29) Stoll, S., and Schweiger, A. (2006) EasySpin, a comprehensive software package for spectral simulation and analysis in EPR. *J. Magn. Reson. 178*, 42–55.

(30) Fufezan, C., Zhang, C. X., Krieger-Liszkay, A., and Rutherford, A. W. (2005) Secondary quinone in photosystem II of *Thermosynechococcus elongatus*: Semiquinone-iron EPR signals and temperature dependence of electron transfer. *Biochemistry 44*, 12780–12789.

(31) Stewart, D. H., and Brudvig, G. W. (1998) Cytochrome b_{559} of photosystem II. *Biochim. Biophys. Acta 1367*, 63–87.

(32) de Paula, J. C., Innes, J. B., and Brudvig, G. W. (1985) Electron-transfer in Photosystem II at cryogenic temperatures. *Biochemistry 24*, 8114–8120.

(33) Hanley, J., Deligiannakis, Y., Pascal, A., Faller, P., and Rutherford, A. W. (1999) Carotenoid oxidation in photosystem II. *Biochemistry 38*, 8189–8195.

(34) Faller, P., Fufezan, C., and Rutherford, A. W. (2005) Side-path electron donors: Cytochrome b_{559}, chlorophyll Z and β-carotene. In *Photosystem II: The light-driven water:plastoquinone oxidoreductase* (Wydrzynski, T. J., and Satoh, K., Eds.) pp 347−365, Springer, Dordrecht, The Netherlands.

(35) Faller, P., Rutherford, A. W., and Debus, R. J. (2002) Tyrosine D oxidation at cryogenic temperature in photosystem II. *Biochemistry 41*, 12914–12920.

(36) Nugent, J. H. A., Doetschman, D. C., and Maclachlan, D. J. (1992) Characterization of the multiple EPR line-shapes of iron semiquinones in Photosystem 2. *Biochemistry 31*, 2935–2941.

(37) Joliot, A. (1974) Effect of low-temperature (−30 to −60 °C) on reoxidation of Photosystem 2 primary electron-acceptor in presence and absence of 3-(3,4-dichlorophenyl)-1,1-dimethylurea. *Biochim. Biophys. Acta 357*, 439–448.

(38) Corrie, A. R., Nugent, J. H. A., and Evans, M. C. W. (1991) Identification of EPR Signals from the States $Q_A^{\bullet-}Q_B^{\bullet-}$ and $Q_B^{\bullet-}$ in Photosystem-II from *Phormidium laminosum*. *Biochim. Biophys. Acta 1057*, 384–390.

(39) Chamorovsky, S. K., and Cammack, R. (1982) Effect of temperature on the photo-reduction of center-a and center-b in Photosystem-I, and the kinetics of recombination. *Biochim. Biophys. Acta 679*, 146–155.

(40) Bouges-Bouquet, B. (1973) Electron transfer between the two photosystems in spinach chloroplasts. *Biochim. Biophys. Acta 314*, 250–256.

(41) Velthuys, B. R., and Amesz, J. (1974) Charge accumulation at reducing side of system 2 of photosynthesis. *Biochim. Biophys. Acta 333*, 85–94.

(42) Nakamura, Y., Kaneko, T., Sato, S., Ikeuchi, M., Katoh, H., Sasamoto, S., Watanabe, A., Iriguchi, M., Kawashima, K., Kimura, T., Kishida, Y., Kiyokawa, C., Kohara, M., Matsumoto, M., Matsuno, A., Nakazaki, N., Shimpo, S., Sugimoto, M., Takeuchi, C., Yamada, M., and Tabata, S. (2002) Complete genome structure of the thermophilic cyanobacterium *Thermosynechococcus elongatus* BP-1. *DNA Res. 9*, 123–130.

(43) Hughes, J. L., Cox, N., Rutherford, A. W., Krausz, E., Lai, T. L., Boussac, A., and Sugiura, M. (2010) D1 protein variants in Photosystem II from *Thermosynechococcus elongatus* studied by low temperature optical spectroscopy. *Biochim. Biophys. Acta 1797*, 11–19.

(44) Kos, P. B., Deak, Z., Cheregi, O., and Vass, I. (2008) Differential regulation of *psbA* and *psbD* gene expression, and the role of the different D1 protein copies in the cyanobacterium *Thermosynechococcus elongatus* BP-1. *Biochim. Biophys. Acta 1777*, 74–83.

(45) Loll, B., Broser, M., Kos, P. B., Kern, J., Biesiadka, J., Vass, I., Saenger, W., and Zouni, A. (2008) Modeling of variant copies of subunit D1 in the structure of photosystem II from *Thermosynechococcus elongatus*. *Biol. Chem. 389*, 609–617.

(46) Thompson, L. K., and Brudvig, G. W. (1988) Cytochrome-b559 may function to protect Photosystem-II from photoinhibition. *Biophys. J. 53*, A269–A269.

(47) Klimov, V. V., Dolan, E., Shaw, E. R., and Ke, B. (1980) Interaction between the intermediary electron-acceptor (pheophytin) and a possible plastoquinone-iron complex in photosystem II reaction centers. *Proc. Natl. Acad. Sci. U.S.A. 77*, 7227–7231.

(48) Sanakis, Y., Petrouleas, V., and Diner, B. A. (1994) Cyanide binding at the non-heme Fe^{2+} of the iron-quinone complex of Photosystem II at high concentrations cyanide converts the Fe^{2+} from high (S=2) to low (S=0) spin. *Biochemistry 33*, 9922–9928.

(49) Deligiannakis, Y., Jegerschold, C., and Rutherford, A. W. (1997) EPR and ESEEM study of the plastoquinone anion radical $Q_A^{-\bullet}$ in photosystem II treated at high pH. *Chem. Phys. Lett. 270*, 564–572.

(50) Astashkin, A. V., Kawamori, A., Kodera, Y., Kuroiwa, S., and Akabori, K. (1995) An electron-spin echo envelope modulation study of the primary acceptor quinone in Zn-substituted plant Photosystem II. *J. Chem. Phys. 102*, 5583–5588.

(51) Tang, X. S., Peloquin, J. M., Lorigan, G. A., Britt, R. D., and Diner, B. A. (1995) The binding environment of the reduced primary quinone electron acceptor, Q_A^{-}, of PSII. *Photosynthesis: From Light to Biosphere*, Vol. I, pp 775−778, Springer, Dordrecht, The Netherlands.